Safety, Reliability, Risk and Life-Cycle Performance of Structures & Infrastructures – Deodatis, Ellingwood & Frangopol (Eds)
© 2013 Taylor & Francis Group, London, ISBN 978-1-138-00086-5

Inference on maximum structural response based on measured accelerations using dynamic Bayesian network

I. Tien
University of California, Berkeley, USA

M. Pozzi
Carnegie Mellon University, USA

A. Der Kiureghian
University of California, Berkeley, USA

ABSTRACT: A Dynamic Bayesian Network (DBN) is a useful tool for analyzing uncertain systems that evolve with time. As such, it is useful in structural health monitoring applications where measurements can be noisy and uncertain. We propose an algorithm that uses a DBN formulation of the system to assess the maximum response of a structure under seismic load, given recordings from accelerometers placed on the structure. By investigating the impact on the accuracy of the sensor characteristics, including the number of sensors, their positions within the structure, and the precision of their measurements, the results of our analysis inform decision making on the use of accelerometers in the monitoring of structures under seismic loads. We assume linear Gaussian response, which is appropriate for serviceability studies. An example application demonstrates that the DBN is a powerful tool for processing of information gained from monitoring devices.

1 INTRODUCTION

A dynamic Bayesian network (DBN) is a statistical tool used to perform prediction and inference in systems evolving with time. The Kalman smoother (KS) is a classical framework for processing of dynamic data in linear Gaussian models, which can be represented as a DBN. In this paper, we apply the KS to model the response of a structure under seismic excitation. Our goal is to infer the maximum response during the earthquake, considering limited prior knowledge on the ground motion and recordings of accelerometers mounted on the structure. This analysis is useful for structural health monitoring applications and informs decision making regarding the use of accelerometer measurements in structures under seismic load.

We assume the excitation to the system is a combination of an earthquake-induced ground motion and noise from ambient vibrations. The earthquake ground acceleration is modeled as a filtered, modulated white-noise process and the dynamical system is idealized as a cascaded system consisting of the ground motion filter and the structure. Sensors mounted on selected floors of the structure record the acceleration with some measurement error. Our method allows for the manager of the structure to tune the stochastic model of the ground motion to the earthquake magnitude and distance, which are assumed to become known shortly after the event. The DBN processes the accelerometer measurements to infer the maximum response of interest.

The proposed formulation allows not only inference on the relative displacements and velocities of the structure at each instant of time, but also the maximum of the structural response during the seismic event. Specifically, we use the KS to infer the joint probability distribution of displacement and velocity responses at each time step. This information is necessary to accurately estimate the distribution of the maximum response.

An application of the proposed algorithm is presented using a shear-type multi-story building model, with the goal of estimating the maximum inter-story drift. We utilize analytical formulas and Monte Carlo simulations to obtain and compare the distributions of maximum inter-story drifts under seismic load. We investigate the influence on the accuracy of the estimation of the number of sensors, their positions within the structure, and the precision of their measurements. The present application is limited to linear structural behavior to allow use of Gaussian models and KS. As such, it is appropriate for operating basis seismic events. Future studies will consider nonlinear behavior.

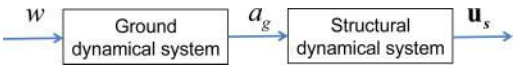

Figure 1. Dynamical system model, consisting of ground and structural dynamical sub-systems.

2 FORMULATION OF THE METHOD

We first model the dynamical system as a cascaded system of two dynamical sub-systems: a ground dynamical system and a structural dynamical system (Figure 1). The ground dynamical sub-system takes a modulated white-noise input w, representing the motion at the bedrock, and outputs the acceleration a_g on the ground surface. The structural dynamical sub-system takes a_g as excitation and produces the structural response $\mathbf{u}_s$, the vector of nodal displacements relative to the ground.

In the following, a capital bold letter denotes a matrix, as $\mathbf{M}$, a small bold letter denotes a vector, as in $\mathbf{u}_s$, and a small italic letter denotes a scalar quantity, as in u_g. Displacement and acceleration are denoted u and a, respectively, while $\mathbf{z}$ includes displacement and velocity. Subscripts *gands* indicate quantities for the ground and structure, respectively.

2.1 *Structural dynamical sub-system*

The equations of motion for the structure subjected to base motion is

$$\mathbf{M}\ddot{\mathbf{u}}_s + \mathbf{C}\dot{\mathbf{u}}_s + \mathbf{K}\mathbf{u}_s = -\mathbf{M}\mathbf{1}a_g + \mathbf{f} \tag{1}$$

where $\mathbf{M}$, $\mathbf{C}$, and $\mathbf{K}$ denote the mass, damping, and stiffness matrices, respectively. $\mathbf{f}$ models a random external force that represents both ambient vibrations and the uncertainty in the external force distribution during the seismic event. In first-order form, using $\mathbf{z}_s^T = [\mathbf{u}_s^{\mathrm{T}} \quad \dot{\mathbf{u}}_s^{\mathrm{T}}]$, equation (1) becomes:

$$\dot{\mathbf{z}}_s = \begin{bmatrix} \mathbf{0} & \mathbf{I} \\ -\mathbf{M}^{-1}\mathbf{K} & -\mathbf{M}^{-1}\mathbf{C} \end{bmatrix} \mathbf{z}_s + \begin{bmatrix} \mathbf{0} \\ -\mathbf{1} \end{bmatrix} a_g + \begin{bmatrix} \mathbf{0} \\ \mathbf{M}^{-1} \end{bmatrix} \mathbf{f} \tag{2}$$

2.2 *Ground dynamical sub-system*

The equation describing the motion on the ground surface relative to the bedrock is given by

$$\ddot{u}_g + 2\xi_g\omega_g\dot{u}_g + {\omega_g}^2 u_g = -w \tag{3}$$

where ω_g and ξ_g define the frequency and damping ratio of the ground filter and w denotes the modulated white-noise acceleration at the bedrock. Written in first-order form with $\mathbf{z}_g = \begin{bmatrix} u_g & \dot{u}_g^{\mathrm{T}} \end{bmatrix}$, equation (3) becomes

$$\dot{\mathbf{z}}_g = \begin{bmatrix} 0 & 1 \\ -{\omega_g}^2 & -2\xi_g\omega_g \end{bmatrix} \mathbf{z}_g + \begin{bmatrix} 0 \\ -1 \end{bmatrix} w \tag{4}$$

The total acceleration at the surface of the ground, a_g, is obtained as

$$\begin{aligned} a_g &= \ddot{u}_g + w = [0 \quad 1]\dot{\mathbf{z}}_g + w \\ &= \begin{bmatrix} -{\omega_g}^2 & -2\xi_g\omega_g \end{bmatrix} \mathbf{z}_g \end{aligned} \tag{5}$$

2.3 *State-space representation*

Combining equations (2), (4) and (5), we obtain a representation of the full dynamical system in first-order form. Defining the system state vector as $\mathbf{z}^T = [\mathbf{z}_g^{\mathrm{T}} \quad \mathbf{z}_s^{\mathrm{T}}]$, we have

$$\begin{aligned} \dot{\mathbf{z}} = &\begin{bmatrix} 0 & 1 & \mathbf{0} & \mathbf{0} \\ -{\omega_g}^2 & -2\xi_g\omega_g & \mathbf{0} & \mathbf{0} \\ \mathbf{0} & \mathbf{0} & \mathbf{0} & \mathbf{I} \\ \mathbf{1}{\omega_g}^2 & 12\xi_g\omega_g & -\mathbf{M}^{-1}\mathbf{K} & -\mathbf{M}^{-1}\mathbf{C} \end{bmatrix} \mathbf{z} \\ &+ \begin{bmatrix} 0 \\ -1 \\ \mathbf{0} \\ \mathbf{0} \end{bmatrix} w + \begin{bmatrix} \mathbf{0} \\ \mathbf{0} \\ \mathbf{0} \\ \mathbf{M}^{-1} \end{bmatrix} \mathbf{f} \end{aligned} \tag{6}$$

Consistent with previous studies (e.g., Gasparini et al. 1983), we define the matrix $\mathbf{A}_c$ and vector $\mathbf{b}_c$ in a state-space representation of the system in continuous time such that $\dot{\mathbf{z}} = \mathbf{A}_c\mathbf{z} + \mathbf{b}_c w + \mathbf{B}_c\mathbf{f}$. Discretizing in time domain in the state-space framework requires the standard transformation $\mathbf{A}_d = e^{\mathbf{A}_c\Delta t}$, $\mathbf{b}_d = \mathbf{A}_c^{-1}(\mathbf{A}_d - \mathbf{I})\,\mathbf{b}_c$, and $\mathbf{B}_d = \mathbf{A}_c^{-1}(\mathbf{A}_d - I)\,\mathbf{B}_c$ (as in Bernal 2007). This leads to

$$\mathbf{z}_{k+1} = \mathbf{A}_d\mathbf{z}_k + \mathbf{b}_d w_k + \mathbf{B}_d\mathbf{f}_k \tag{7}$$

as the full equation of motion for the system in discrete time step k. For the sake of simplicity, hereafter we drop the subscripts d and write the discretized equation as $\mathbf{z}_{k+1} = \mathbf{A}\mathbf{z}_k + \mathbf{b}w_k + \mathbf{B}\mathbf{f}_k$.

2.4 *Modeling the excitation*

To represent the non-stationarity of ground motion, we model the acceleration at the bedrock as a modulated, band-limited white-noise process. Thus, w is normally distributed with zero mean and a time-varying variance $\sigma_w^2(t)$. Following Rezaeian and Der Kiureghian (2010), $\sigma_w^2(t)$ is taken as proportional to a gamma probability density function (PDF). The gamma PDF is a reasonable model for this purpose, since it is non-negative, starts and ends at zero, and the shape is skewed with a longer right tail, which is typical of earthquake motions. The parameters of the gamma PDF are determined in terms of descriptive variables of the seismic event. Specifically, we take the mode of the distribution to coincide with the time of the maximum intensity of the ground motion, t_{eq}^{max}, and the middle 90% of the distribution to represent the effective duration of the earthquake motion, D_{5-95}, which we define as the time between 5% and 95% Arias intensity values. These modeling assumptions lead to the shape and scale parameters of the gamma distribution

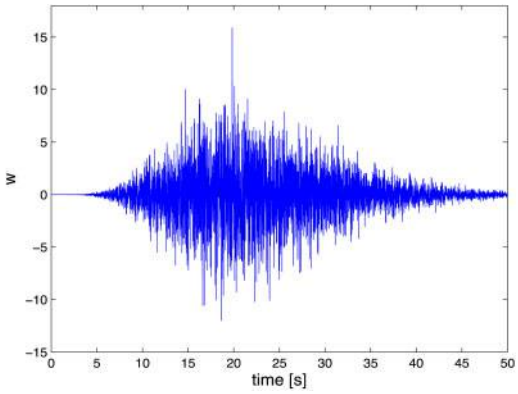

Figure 2. Bedrock excitation w with time-varying variance $\sigma_w^2(t)$ proportional to the gamma PDF.

as $k = \frac{t_{eq}^{max}}{\theta} + 1$ and $\theta = -\frac{1}{2}t_{eq}^{max} + \frac{1}{4}\sqrt{4t_{eq^{max}}^2 + D_{5-95}^2}$, respectively. The distribution is scaled by a factor to achieve the desired intensity of the motion. Figure 2 shows a realization of a modulated white noise with $t_{eq}^{max} = 20$ sec, $D_{5-95} = 25$ sec, and a scale factor of 200. For this example, the discretization time step is set as $\Delta t = 0.01$ sec. This effectively cuts frequencies off at 50 Hz.

2.5 *System evolution*

Given the state-space representation of the system, the system evolution from time step k to $k+1$ is described as in equation (7). We take $\mathbf{f}_k$ to be normally distributed with zero mean and covariance matrix $\sigma_f^2\mathbf{I}$, with statistically independent values for different time steps and for different degrees of freedom. Including this additional force increases the uncertainty in our model.

2.6 *Observation equation*

We assume sensors measure the total acceleration of the structure, which is given by

$$\mathbf{a}_t = \ddot{\mathbf{u}}_s + \mathbf{1}a_g \tag{8}$$

From equation (1) and $\mathbf{z}$ as defined in (6), we obtain:

$$\begin{aligned}\mathbf{a}_t &= -\mathbf{M}^{-1}\mathbf{K}\mathbf{u}_s - \mathbf{M}^{-1}\mathbf{C}\dot{\mathbf{u}}_s + \mathbf{M}^{-1}\mathbf{f} \\ &= -\mathbf{M}^{-1}[\mathbf{0} \quad \mathbf{0} \quad \mathbf{K} \quad \mathbf{C}]\mathbf{z} + \mathbf{M}^{-1}\mathbf{f}\end{aligned} \tag{9}$$

Let $\mathbf{S}$ define a matrix that selects the degrees of freedom where accelerometers are placed. The observation equation at each time step k is then given by

$$\mathbf{y}_k = \mathbf{D}\mathbf{z}_k + \boldsymbol{\nu}_k + \mathbf{S}\mathbf{M}^{-1}\mathbf{f}_k \tag{10}$$

where $\mathbf{D} = -\mathbf{S}\mathbf{M}^{-1}[\mathbf{0} \quad \mathbf{0} \quad \mathbf{K} \quad \mathbf{C}]$ is the observation matrix.

We take the measurement error $\boldsymbol{\nu}_k$ to be normally distributed with zero mean and time-independent variance σ_ν^2, and, again, we assume errors at different times are independent.

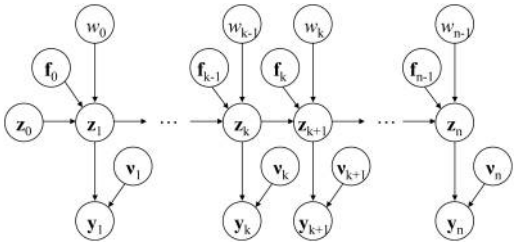

Figure 3. Representation of system as a DBN.

2.7 *Dynamic Bayesian network (DBN)*

The system to be analyzed is represented by the DBN shown in Figure 3. The DBN consists of a sequence of BNs, each representing the system at a slice in time, $1, \ldots, n$. Terms with zero indices represent initial values at time zero, which are also uncertain. We use the Kalman filter approach as described below to process the information in the DBN.

2.8 *Kalman filter (KF)*

To estimate the state of the system $\boldsymbol{z}$ taking into account measurements y, we use a Kalman filter (KF) approach. Using equation (6), we predict the mean vector and covariance matrix of the system state at step k as

$$\boldsymbol{\mu}_{\mathbf{Z}_k}{}^{P} = \mathbf{A}\boldsymbol{\mu}_{\mathbf{Z}_{k-1}} \tag{11}$$

$$\boldsymbol{\Sigma}_{\mathbf{Z}_k\mathbf{Z}_k}{}^{P} = \mathbf{A}\boldsymbol{\Sigma}_{\mathbf{Z}_{k-1}\mathbf{Z}_{k-1}}\mathbf{A}^{\mathrm{T}} + \boldsymbol{\Sigma}_{\mathrm{E}_k} \tag{12}$$

where $\boldsymbol{\Sigma}_{\mathrm{E}_k} = \mathbf{b}\sigma_{w_k}^2\mathbf{b}^{\mathrm{T}} + \boldsymbol{\Sigma}_\varepsilon^2$. We then calculate:

$$\mathbf{e}_k = \mathbf{y} - \mathbf{D}\boldsymbol{\mu}_{\mathbf{Z}_k}{}^{P} \tag{13}$$

$$\mathbf{R}_k = \mathbf{D}\boldsymbol{\Sigma}_{\mathbf{Z}_k\mathbf{Z}_k}{}^{P}\mathbf{D}^{\mathrm{T}} + \sigma_\nu{}^2\mathbf{I} \tag{14}$$

$$\mathbf{K}_{G_k} = \boldsymbol{\Sigma}_{\mathbf{Z}_k\mathbf{Z}_k}{}^{P}\mathbf{D}^{\mathrm{T}}\mathbf{R}_k{}^{-1} \tag{15}$$

$\mathbf{e}_k$ is known as the innovation, $\mathbf{R}_k$ characterizes the uncertainty due to the measurement error, and $\mathbf{K}_{G_k}$ is the Kalman gain matrix (Welch and Bishop 1995). The innovation measures the difference between the measurements and the predicted mean values. The Kalman gain takes into account the accuracy of the observations to provide a weight on measurement information compared to the prediction in updating the estimates. Thus, the mean vector and covariance matrix of the system state are updated as

$$\boldsymbol{\mu}_{\mathbf{Z}_k} = \boldsymbol{\mu}_{\mathbf{Z}_k}{}^{P} + \mathbf{K}_{G_k}\mathbf{e}_k \tag{16}$$

$$\boldsymbol{\Sigma}_{\mathbf{Z}_k\mathbf{Z}_k} = (\mathbf{I} - \mathbf{K}_{G_k}\mathbf{D})\boldsymbol{\Sigma}_{\mathbf{Z}_k\mathbf{Z}_k}{}^{P} \tag{17}$$

2.9 *Kalman smoother (KS)*

The KF performs a forward pass through the data to update the estimates of the system state as information from measurements becomes available. Once we have information over a fixed time interval, we can perform a backward pass through the data to further update our estimates using the Kalman smoother (KS) (Murphy 2002). To apply the KS, we first compute the smoother gain matrix:

$$\mathbf{J}_k = \mathbf{\Sigma}_{Z_k Z_k} \mathbf{A}^{\mathrm{T}} \left(\mathbf{\Sigma}_{Z_{k+1} Z_{k+1}}{}^{P} \right)^{-1} \tag{18}$$

We then update our estimates:

$$\boldsymbol{\mu}_{Z_k}{}^{KS} = \boldsymbol{\mu}_{Z_k} + \mathbf{J}_k \left(\boldsymbol{\mu}_{Z_{k+1}}{}^{KS} - \boldsymbol{\mu}_{Z_{k+1}}{}^{P} \right) \tag{19}$$

$$\mathbf{\Sigma}_{Z_k Z_k}{}^{KS} = \mathbf{\Sigma}_{Z_k Z_k} + \mathbf{J}_k \left(\mathbf{\Sigma}_{Z_{k+1} Z_{k+1}}{}^{KS} - \mathbf{\Sigma}_{Z_{k+1} Z_{k+1}}{}^{P} \right) \mathbf{J}_k{}^{\mathrm{T}} \tag{20}$$

It is these final estimates of the system state from applying the KS that we use to assess the maximum response of the system.

2.10 *Distribution of the maximum response*

Let $Z(t)$ be a linear function of system state $\mathbf{z}_s$. We are interested in the probability of the nonstationary process $Z(t)$ exceeding a given threshold ζ during an interval $(0, T)$, where T is the duration of the response. We begin with the equation for the extreme value $Z_{\max} = \max_t Z(t)$ of a nonstationary process:

$$\begin{aligned} P(Z_{max} > \zeta) &= 1 - P(Z_{max} \leq \zeta) \\ &\cong 1 - \exp\left[- \int_0^T \nu(\zeta^+, t) dt \right] \end{aligned} \tag{21}$$

where $\nu(\zeta^+, t)$ is the mean ζ-level up-crossing rate and T is the duration of the response. The approximation is based on an assumption of Poisson crossings and is valid for high thresholds. Due to conditioning on observed responses, $Z(t)$ is no longer a zero-mean process. Thus, to obtain $\nu(\zeta^+, t)$, we cannot use the well-known formula for up-crossings of zero-mean nonstationary Gaussian processes (Rice 1944). Instead, we define the process $X(t) = Z(t) - \mu_Z(t)$, where $X(t)$ is a zero-mean process with $\sigma_X(t) = \sigma_Z(t)$. We use the fact that the up-crossings of the non-zero-mean process $Z(t)$ above a fixed threshold ζ are identical to the up-crossings of the zero-mean process $X(t)$ above a time-varying threshold $\eta(t) = \zeta - \mu_Z(t)$ to obtain

$$\nu(\zeta^+, t) = \nu_{\dot{X}}(\eta(t)^+, t) = \int_{\dot{\eta}}^{\infty} (\dot{x} - \dot{\eta}) f_{X\dot{X}}(\eta, \dot{x}, t) d\dot{x} \tag{22}$$

in which

$$f_{X\dot{X}}(\eta, \dot{x}, t) = \frac{1}{2\pi \sigma_X \sigma_{\dot{X}} \sqrt{1-\rho^2}} \exp\left[- \frac{1}{2(1-\rho^2)} \left(\frac{\eta^2}{\sigma_X^2} - 2\rho \frac{\eta \dot{x}}{\sigma_X \sigma_{\dot{X}}} + \frac{\dot{x}^2}{\sigma_{\dot{X}}^2} \right) \right] \tag{23}$$

wherein $\eta(t)$, $\sigma_X(t)$, $\sigma_{\dot{X}}(t)$ and $\rho = \rho_{\dot{X}(t)X(t)}$ are all functions of time. Using equations (22) and (21), after some derivations, one obtains

$$\begin{aligned} \nu_X(\eta(t)^+, t) = \frac{\exp\left[-\frac{1}{2} \frac{\eta^2}{\sigma_X^2} \right]}{2\pi \sigma_X \sigma_{\dot{X}} \sqrt{1-\rho^2}} \Bigg\{ & \sigma_{\dot{X}}^2 (1 - \rho^2) \exp\left[- \frac{r^2}{2\sigma_{\dot{X}}^2 (1-\rho^2)} \right] \\ & + \sqrt{2\pi (1-\rho^2)} \sigma_{\dot{X}} \left[1 - \Phi\left(\frac{r}{\sigma_{\dot{X}} \sqrt{1-\rho^2}} \right) \right] \left(\frac{\sigma_{\dot{X}} \rho \eta}{\sigma_X} - \dot{\eta} \right) \Bigg\} \end{aligned} \tag{24}$$

where $r = \dot{\eta} - \frac{\rho \eta \sigma_{\dot{X}}}{\sigma_X}$ and $\Phi(\cdot)$ indicates the normal CDF. Using equations (21) and (24), we obtain an approximation of the CDF of the maximum response Z_{max}.

2.11 *Application*

As an example of the proposed algorithm, we consider a 10-story shear-type building with uniform mass and stiffness, as shown in Figure 4. The parameters of the structure are set such that the fundamental period of the structure is 1 sec. We take the stochastic excitation at the bedrock level as described for the example realization in Figure 2, and the set the parameters of the ground filter as $\omega_g / 2\pi = 1.5$ Hz and $\xi_g = 0.4$. The ratio of $\sigma_f / \sigma_w(t_{max})$ is set at 0.3. The response we are interested in is the inter-story drift between floors 4 and 5.

3 RESULTS

To investigate the accuracy of our approach, we simulate the seismic event and the ambient noise. We compute the structural response from this generated combined excitation, and we call this the "actual" response. We then simulate measurements of this response, including measurement noise. These are the observations that we obtain from the accelerometers mounted on the structure. Then, assuming we have only these noisy measurements of floor accelerations, we use our DBN formulation of the system to estimate the response of the structure to the seismic loading.

In the results presented in this section, we first analyze the effect of the KS in improving the predictions by KF. Next, we investigate the influence on the accuracy of the estimation of varying the characteristics of the measurements used in the analysis, including the number of sensors, their positions within the structure, and the precision of their measurements. Finally, we compare the results we obtain from the analytical solution to those from the Monte Carlo simulations to analyze the distribution of the maximum response.

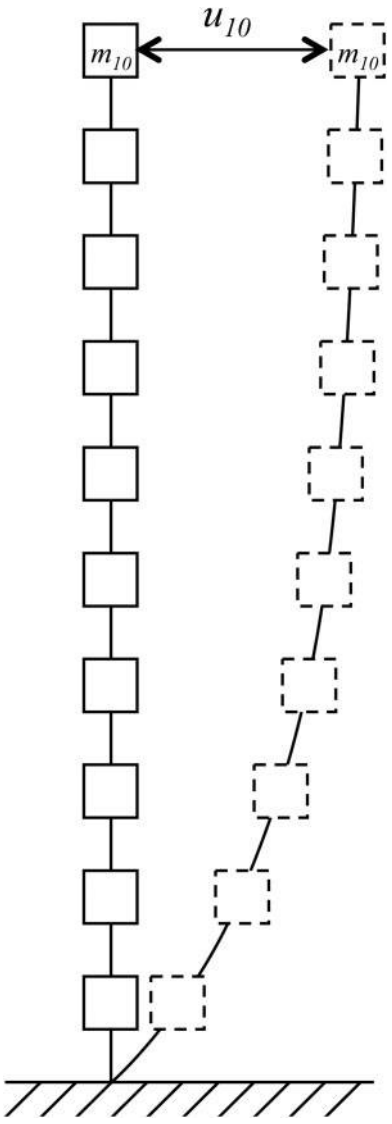

Figure 4. 10-story shear-type building model.

3.1 *KF vs. KS*

With one sensor placed on the top floor of the building, Figure 5 shows the resulting estimates of the inter-story drift #5 compared to the simulated "actual" values, using the KF versus the KS. The standard deviation of measurement error is set at $\sigma_v = 0.5$ m/s^2. Because the time histories are close, Figure 6 shows the results for one particular peak that occurs at $t = 19$ sec. Any other segment of the time history can similarly be chosen to analyze the results of the estimation. Hereafter, we only examine the segment of the time history around the peak at the above selected time.

Figure 6 shows that, consistent with the theory, employing the KS improves the accuracy of the estimate of the inter-story drift compared to using only the KF. Utilizing the additional information of the measurements over the entire time history results in a KS mean estimate that is closer to the actual inter-story drift values and a decreased variance in the estimate, resulting in a narrower-banded estimate.

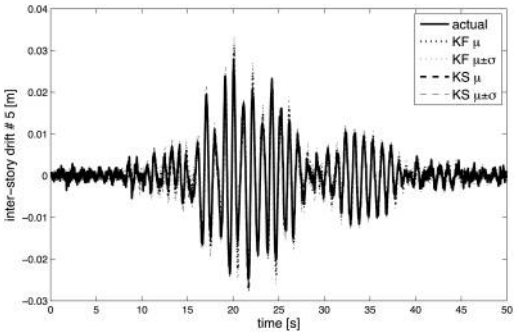

Figure 5. Estimate of the inter-story drift #5 using the KF versus the KS.

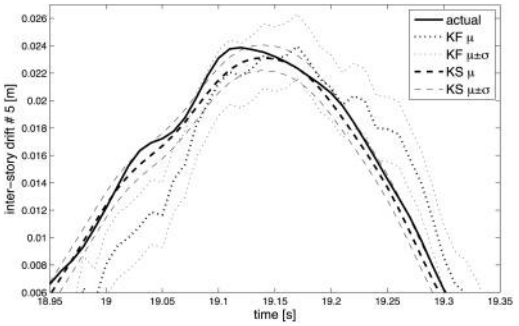

Figure 6. Estimate of the inter-story drift using the KF versus the KS, for the peak at $t = 19$ sec.

3.2 *Varying measurement characteristics*

Figure 7 shows the mean KS estimates compared to the actual inter-story drift values, as indicated by the solid line, based on measurements from sensors placed in varying configurations on the structure. The estimates from one sensor placed on the bottom of the structure at floor 1, from one sensor placed at the top of the structure at floor 10, and from four sensors placed at floors 1, 4, 7, and 10, are indicated by the dotted, dash-dot, and dashed lines, respectively. Figure 8 shows the standard deviations of the KS estimates over the entire duration of the loading using the same sensor configurations.

Figure 7 shows that more information results in more accurate estimates of the response. The mean estimate of inter-story drift utilizing the measurements from four sensors placed on the structure is more accurate than the estimates that utilize measurements from only one sensor. However, looking at the results of using only one sensor, we see that the placement of the sensor also matters. Because we are looking at the

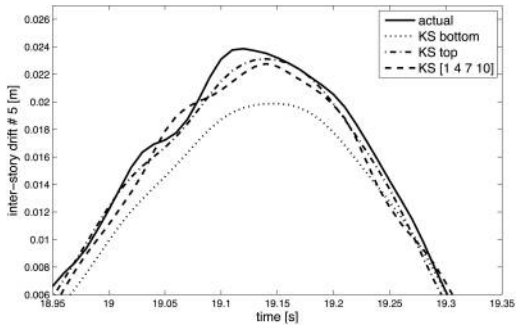

Figure 7. Mean KS estimates of the inter-story drift for varying sensor number and placement, peak at $t = 19$ sec.

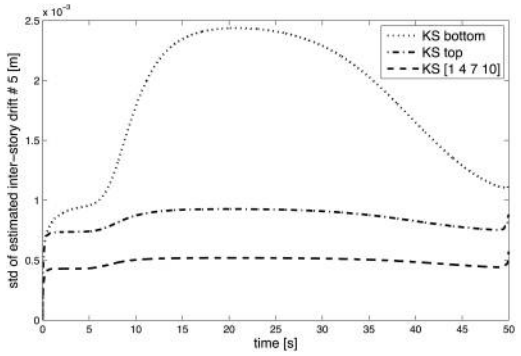

Figure 8. Standard deviations of KS-estimated inter-story drift for varying sensor number and placement.

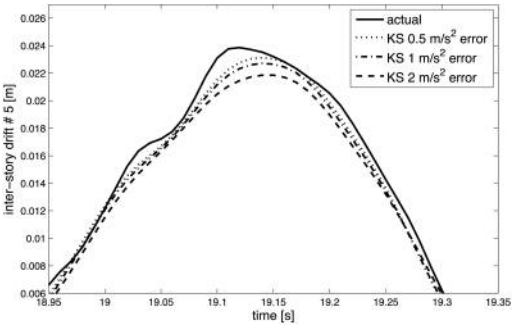

Figure 9. Mean KS estimates of the inter-story drift varying sensor precision, peak at $t = 19$ sec.

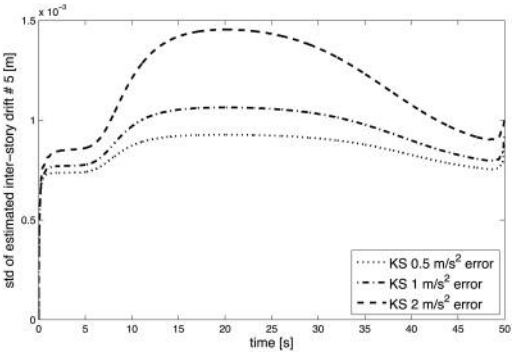

Figure 10. Standard deviations of KS-estimated inter-story drift varying sensor precision.

inter-story drift at floor 5 where no direct measurements are being made, the sensors at the bottom and top of the structure on floors 1 and 10, respectively, are equally far from the response of interest. The accuracy of the corresponding drift estimates, however, are not equal. The mean estimate using the information from the top sensor is more accurate than the mean estimate using the information from the bottom sensor. Correspondingly, in Figure 8, the standard deviations are higher for the estimate that uses the sensor at the bottom floor compared to the estimate that uses the sensor at the top floor. Thus, the two figures show that an accelerometer placed at the upper floor of a building instead of the lower floor leads to more accurate estimates of the mean and a smaller variance.

This result is explained by considering the signal-to-noise ratio (SNR). The amplitude of the floor acceleration in response to a seismic excitation is higher at the higher floors, so with the same device, the SNR is higher for measurements at the higher floors. Therefore, if given the choice, one would prefer to place accelerometers at the upper floors of a building instead of the lower floors, to obtain measurements that are more informative regarding the structural response and will result in more accurate estimates of the system state.

Figure 9 shows the mean KS estimates compared to the actual inter-story drift values, as indicated by the solid line, using measurements from one sensor placed at the top of the structure at floor 10. This time, we vary the precision of the sensors such that the measurements are made with 0.5 m/s^2, 1 m/s^2, and 2 m/s^2 error, as indicated by the dotted, dash-dot, and dashed lines, respectively. Figure 10 shows the standard deviations of the KS estimates for the entire duration of loading using of the same three levels of precision as in Figure 9.

Figure 9 shows that more precise sensors result in more accurate mean estimates of the system state, and Figure 10 shows that increasing the precision of the sensors reduces the variance of the estimate, although the effect is not large. Improving the sensor by 4 times, i.e., reducing the error in the measurement from 2 m/s^2 to 0.05 m/s^2, only reduces the average standard deviation of the estimate by about 30%, from 12×10^{-4} m to 8.5×10^{-4} m. In contrast, reexamining Figure 8, we see that changing the placement of the same single sensor from the bottom of the structure to the top of the structure reduces the average standard deviation of the estimate by more than half, from 18×10^{-4} m to 8.5×10^{-4} m.

Finally, to compare the accuracy of the estimates across different combinations of sensor number, placement, and precision, Figure 11 shows the maximum root mean square errors (RMSE's) of the mean KS estimates of the inter-story drift using one sensor at

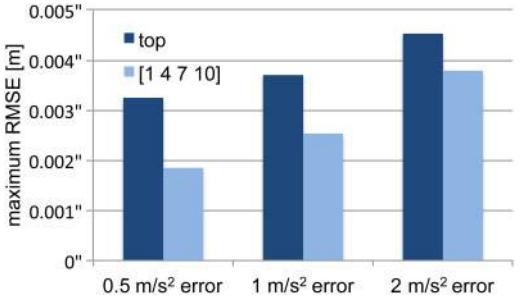

Figure 11. RMSE's of KS-estimated inter-story drift varying sensor number, placement, and precision.

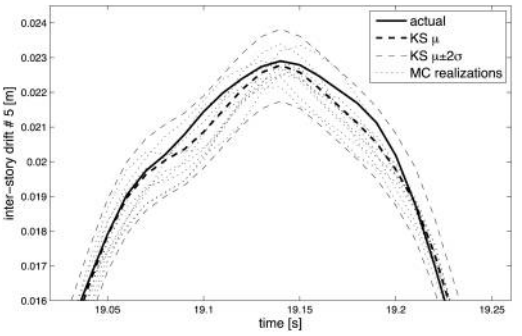

Figure 12. KS-estimated compared to MC realizations of inter-story drift, peak at $t = 19$ sec.

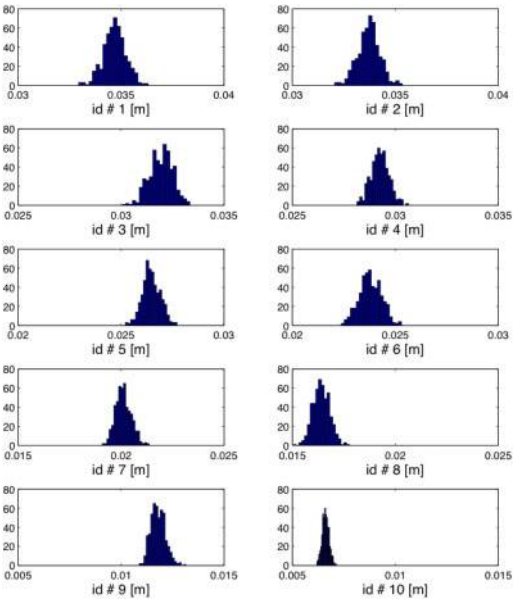

Figure 13. Distributions of the maximum inter-story drift from MC simulations for all 10 degrees of freedom of the structure.

the top floor compared to four sensors at floors 1, 4, 7, and 10, and with varying precisions of 0.5 m/s^2, 1 m/s^2, and 2 m/s^2 error. Placing one sensor at the bottom floor results in a maximum RMSE of .0059 m, significantly higher in magnitude than the results for the sensor at the top floor and for the four sensors, and therefore is not shown.

Figure 11 shows that keeping sensor precision constant, placing four sensors on the building compared to placing one on the top floor reduces the maximum RMSE of the estimate by about 20% for the 2 m/s^2 error sensor, 30% for the 1 m/s^2 error sensor, and 40% for the 0.5 m/s^2 error sensor. In addition, the maximum RMSE of mounting four sensors of lesser quality throughout the building is larger compared to mounting one sensor of higher quality at the top floor of the building. When comparing these two monitoring strategies, an additional consideration to the accuracy of the estimation of the system state is the reliability of the structural health monitoring device. Assuming equal device reliability, a monitoring system of four sensors will be more robust to sensor device failure than a system comprised of only one sensor.

3.3 *Distribution of the maximum*

Using the KS-estimated distribution of the system state using the measurements from four sensors of precision 0.5 m/s^2 error placed one each at floors 1, 4, 7, 10, we generate MC realizations of the process. Each MC realization produces a time history of the inter-story drift. Figure 12 randomly selects 10 of these realizations for plotting to compare to the KS estimates. The thick solid line indicates the actual inter-story drift values, the thick dashed line indicates the KS-estimated mean, and the thin dashed lines indicate the KS mean +/− two standard deviations. The dotted lines indicate the MC realizations. Taking the maximum of the inter-story drift over the time period of analysis, Figure 13 shows the distributions of the maximum inter-story drift for all 10 degrees of freedom of the structure.

In analyzing the distribution of the maximum response, Figure 12 shows the MC realizations to lie within the mean estimate of the response +/− two standard deviations. Figure 13 shows the distributions of the maximum inter-story drift for all stories. These results enable us to obtain statistics of the maximum inter-story drift for each story of the structure. We note that the dispersions in these distributions are rather small in spite of the stochastic nature of the excitation. This is due to the conditioning on the measured acceleration response.

In analyzing the distribution of the maximum response, we also look at the probability that the maximum response will exceed a certain threshold level. From both the analytical solution and MC simulations, we obtain a complementary CDF that shows this probability of exceedance. The analytical solution uses the approximation in Eq. (21), which is valid for high thresholds and low probabilities of exceedance, and the CDF's from MC are the empirical CDF's. Figure 14 compares the complementary CDF's for all 10 degrees

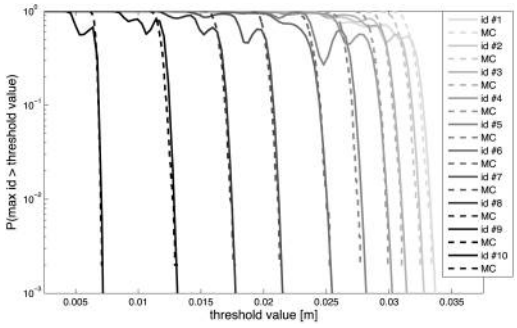

Figure 14. Complementary CDF of maximum inter-story drift: analytical vs. MC.

of freedom obtained from these two methods of analysis. The plot shows the probability of the maximum inter-story drift exceeding a threshold as a function of threshold value. The probabilities of exceedance are on the y-axis on a logarithmic scale, and the threshold values are on the x-axis. The solid lines indicate the results from the analytical solution, and the dotted lines indicate the results from MC.

In Figure 14, we see that the results from the analytical solution and MC are most consistent at high degrees of freedom. At the upper floors of the structure, the acceleration response is higher, leading to more accurate estimates. In addition, the analytical results display a phenomenon that we know cannot be true, namely a non-monotonically decreasing complementary CDF for the probability that the maximum response exceeds a threshold as a function of threshold value, at high probabilities of exceedance. This is due to the approximation made in Eq. (21). The approximation assumes Poisson crossings of the process above the threshold, and therefore is only valid for high thresholds. The results in Figure 14 show this to be the case. The anomalies in the analytical solution occur at probabilities of exceedance above 0.25.

This result shows the limitations of the Poisson crossings assumption in analyzing extreme values. The analytical solution is really only valid for high thresholds and low probabilities of exceedance. It is at these high thresholds where damage occurs and it is the structural response in this range that we are interested in for our analysis. Therefore, focusing on these high thresholds, we see close agreement between the complementary CDFs at probabilities of exceedance below 0.1 for all degrees of freedom. Figure 14 shows that our methodology enables us to assess the maximum response of a structure to seismic load and estimate the probability that the maximum response will exceed a high threshold.

4 CONCLUSION

We have developed a methodology that uses the DBN framework to analyze the maximum response of a structure to seismic loading based on measured accelerations. Investigating the influence of various sensor characteristics on the accuracy of the estimation, we show that sensor placement has a more significant effect than sensor precision. Sensors placed at the top of a structure are more informative than sensors placed at the bottom, and while increasing the precision of the sensors does improve the estimation, the effect is small.

We have presented an analytical solution to estimate the maximum response, which produces results that are consistent with MC simulations for high thresholds.

The results from our analysis inform decision making on the use of accelerometers mounted on the structure for structural health monitoring applications as well as provide insight on the applicability of analytical formulas to analyze the distribution of the maximum response.

ACKNOWLEDGEMENTS

The first author gratefully acknowledges support from the National Science Foundation Graduate Research Fellowship. Additional support is provided by the National Science Foundation Grant No. CMMI-1130061, which is also gratefully acknowledged.

REFERENCES

Bernal, D., "New approaches to analysis and testing of mechanical and structural systems: state space identification," *Workshop at the International Centre for Mechanical Sciences,* June 18–22, 2007.

Gasparini, D. A. et al., "Random Vibration of Cascaded Secondary System," *Proceedings of the 7th SMIRT Conference*, Chicago, Illinois, pp. 445–451, 1983.

Murphy, K., "Dynamic Bayesian networks: representation, inference and learning," *Doctoral Thesis,* 2002.

Rezaeian, S., and Der Kiureghian, A., "Stochastic Modeling and Simulation of Ground Motions for Performance-Based Earthquake Engineering," *Pacific Earthquake Engineering Research Center (PEER) Report No. 2010/02*, University of California, Berkeley, June 2010.

Rice, S. O., "Mathematical analysis of random noise," *Bell System Technical Journal*, Vol. 23, No. 3, pp. 282–332, July 1944.

Welch, G., and Bishop, G., "An introduction to the Kalman filter," Department of Computer Science, University of North Carolina at Chapel Hill, Technical Report 95-041, 1995.